Article

Nanoparticle-Cored Dendrimers: Synthesis and Characterization

Karical R. Gopidas, James K. Whitesell, and Marye Anne Fox

J. Am. Chem. Soc., **2003**, 125 (21), 6491-6502• DOI: 10.1021/ja029544m • Publication Date (Web): 01 May 2003

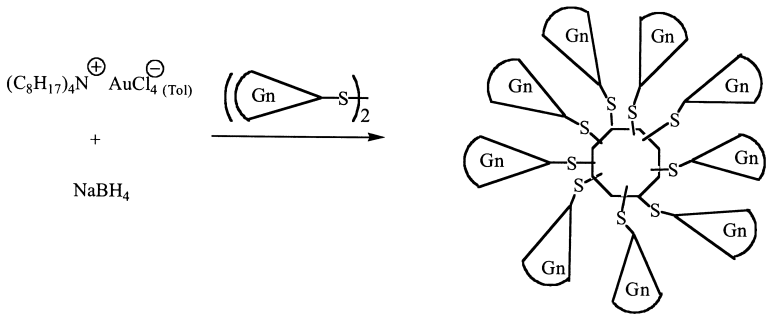

More About This Article

Additional resources and features associated with this article are available within the HTML version:

- Supporting Information
- Links to the 10 articles that cite this article, as of the time of this article download
- Access to high resolution figures
- Links to articles and content related to this article
- Copyright permission to reproduce figures and/or text from this article

View the Full Text HTML

J|A|C|S
ARTICLES
Published on Web 05/01/2003

Nanoparticle-Cored Dendrimers: Synthesis and Characterization

Karical R. Gopidas,† James K. Whitesell,* and Marye Anne Fox*

Contribution from the Department of Chemistry, North Carolina State University, Campus Box 8204, Raleigh, North Carolina 27695

Received December 2, 2002; E-mail: mafox@ncsu.edu

Abstract: The synthesis and characterization of a group of new dendrimers—namely, nanoparticle-cored dendrimers (NCDs)—are described. These materials were obtained by the reduction of hydrogen tetrachloroaurate phase-transferred into toluene in the presence of Fréchet-type polyaryl ether dendritic disulfide wedges of generation 1−5. These materials, possessing nanometer-sized gold clusters at the core and dendritic wedges radially connected to the core by Au−S bonds, were analyzed by TEM and TGA, and by UV, IR, and NMR spectroscopies. The number of branching units connected to the core decreased with the generation of the dendritic wedge, and this number changed from 2.18/nm^2 for Au−G-2 to 0.27/nm^2 for Au−G-5. This result suggests that, in the higher-generation NCDs, a large fraction of the surface area of the metal cluster is not passivated and is therefore available for catalytic activity.

Introduction

Dendrimers, also known as arborols or starburst polymers, are a group of highly ordered, three-dimensional (3D), treelike functional polymers.[1] Since the early work of Tomalia[2] and Newkome[3] in the mid 1980s, there has been a remarkable increase in interest in these aesthetically appealing macromolecules. Dendrimers are monodisperse macromolecules, and they differ from classical random coil polymers in that they possess three distinguishing architectural components, namely (a) an initiator core, (b) interior layers called "generations" (denoted by the letter G) composed of repeating units radially attached to the initiator core, and (c) a layer of terminal groups attached to the outermost branching unit. These components essentially determine the overall size, shape, and physicochemical properties of the dendrimer. Dendrimer size increases linearly and the number of surface functional groups increases exponentially with generation number. The lower-generation dendrimers are approximately flat and open, whereas the higher-generation dendrimers are almost spherical and contain significant interior void spaces. The high density of terminal functional groups in higher-generation dendrimers provides a large number of reactive sites for potential applications such as nanoscale catalysts, micelle mimics, drug delivery agents, and chemical sensors.[4]

Dendrimers are generally synthesized by the "divergent"[1] or "convergent" approaches.[1,5] Both methods have advantages and disadvantages. The divergent approach is suitable for the preparation of large quantities of higher-generation dendrimers, but the dendrimers thus produced will have defects arising from incomplete reactions on the surface. Dendrimers synthesized by the convergent approach will generally have fewer defects, but the synthesis is typically limited to lower generations. The convergent synthesis, however, allows unparalleled control over functionality at specified locations of the dendrimer. It also provides access to numerous novel architectures through the attachment of dendritic branches to other molecules.

Metal-containing dendrimers are materials of current interest. Several reports dealing with the synthesis and characterization of metal-ion-containing dendrimers, dendrimer-encapsulated metal nanoparticles, and dendrimer−metal nanocomposites have

† Permanent address: Photochemistry Research Unit, Regional Research Laboratory (CSIR), Trivandrum û 695 019, India.

(1) (a) Tomalia, D. A.; Naylor, A. M.; Goddard, W. A., III. *Angew. Chem., Int. Ed. Engl*. **1990**, *29*, 138. (b) *Dendrimers IV: Metal Coordination, Self-Assembly, Catalysis*; Topics in Current Chemistry, No. 217; Vögtle, F., Schalley, C. A., Eds.; Springer-Verlag: Berlin, 2001. (c) *Dendrimers III: Design, Dimension, Function*; Topics in Current Chemistry, No. 212; Vögtle, F., Ed.; Springer-Verlag: Berlin, 2001. (d) *Dendrimers and Other Dendritic Polymers*; Fréchet, J. M. J., Tomalia, D. A., Eds.; John Wiley & Sons: Chichester, U.K., 2001. (e) *Dendrimers II: Architecture, Nanostructure and Supramolecular Chemistry*; Topics in Current Chemistry, No. 210; Vögtle, F., Ed.; Springer-Verlag: Berlin, 2000. (f) *Dendrimers*; Topics in Current Chemistry, No. 197; Vögtle, F., Ed.; Springer-Verlag: Berlin, 1998. (g) Newkome, G. R.; Moorefield, C. N.; Vögtle, F. *Dendritic Molecules: Concepts, Synthesis Perspectives*; VCH: New York, 1996.

(2) Tomalia, D. A.; Baker, H.; Dewald, J.; Hall, M.; Kallos, G.; Martin, S.; Roeck, J.; Ryder, J.; Smith, P. *Polym. J*. **1985**, *17*, 117.

(3) Newkome, G. R.; Yao, Z.-Q.; Baker, G. R.; Gupta, V. K. *J. Org. Chem*. **1985**, *50*, 2003.

(4) (a) van Heerbeek, R.; Kamer, P. C. J.; van Leeuwen, P. W. N. M.; Reek, J. N. H. *Chem. Rev*. **2002**, *102*, 3717. (b) Bezouska, K. *Rev. Mol. Biotechnol*. **2002**, *90*, 269. (c) Reek, J. N. H.; de Groot, D.; Oosterom, G. E.; Kamer, P. C. J.; van Leeuwen, P. W. N. M. *Rev. Mol. Biotechnol*. **2002**, *90*, 159. (d) Twyman, L. J.; King, A. S. H.; Martin, I. K. *Chem. Soc. Rev*. **2002**, *31*, 69. (e) Astruc, D.; Chardac, F. *Chem. Rev*. **2001**, *101*, 2991. (f) Tully, D. C.; Fréchet, J. M. J. *Chem. Commun*. **2001**, 1229. (g) Oosterom, G. E.; Reek, J. N. H.; Kamer, P. C. J.; van Leeuwen, P. W. N. M. *Angew. Chem., Int. Ed*. **2001**, *40*, 1828. (h) Shamsi, S. A.; Palmer, C. P.; Warner, I. M. *Anal. Chem*. **2001**, *73*, 140. (i) Duncan, R. *Polym. Mater. Sci. Eng*. **2001**, *84*, 214. (j) Dykes, G. M. *J. Chem. Technol. Biotechnol*. **2001**, *76*, 903. (k) Vögtle, F.; Gestermann, S.; Hesse, R.; Schwierz, H.; Windisch, B. *Prog. Polym. Sci*. **2000**, *25*, 987. (l) Bosman, A. W.; Janssen, H. M.; Meijer, E. W. *Chem. Rev*. **1999**, *99*, 1665.

(5) (a) Grayson, S. M.; Fréchet, J. M. J. *Chem. Rev*. **2001**, *101*, 3819. (b) Hawker, C. J.; Fréchet, J. M. J. *J. Am. Chem. Soc*. **1990**, *112*, 7638. (c) Hawker, C. J.; Fréchet, J. M. J. *Macromolecules*, **1990**, *23*, 4726. (d) Wooley, K. L.; Hawker, C. J.; Fréchet, J. M. J. *J. Chem. Soc., Perkin Trans. 1* **1991**, 1059. (e) Miller, T. M.; Neenan, T. X. *Chem. Mater*. **1990**, *2*, 346. (f) Kwock, E. W.; Neenan, T. X.; Miller, T. M. *Chem. Mater*. **1991**, *3*, 775.

appeared recently.[6] There are three general categories of metal-ion-containing dendrimers. The first category consists of dendrimers with metal ions as an integral part of their structure.[7] Examples include dendrimers that have an organometallic core and those that use metal ligation to assemble the dendrimer branches. The second category consists of dendrimers with peripheral groups that can bind metal ions.[8] Metal-ion binding in these cases can be electrostatic (as in carboxylate-terminated dendrimers) or coordinative (as in terpyridine- or phosphine-terminated dendrimers). The third category consists of dendrimers that encapsulate metal ions.[9] These dendrimers generally contain functional groups that can coordinate to metal ions in their interior. It has been demonstrated recently[10] that metal ions encapsulated in the interior cavities of dendrimers can be reduced chemically, resulting in the formation of dendrimers containing encapsulated metal nanoparticles. The encapsulated nanoparticles are protected from agglomeration by the encasing dendrimer, and a substantial fraction of their surface is non-passivated and available for participation in catalytic reactions. Applications of these dendrimer-encapsulated metal nanoparticles in catalysis have been well demonstrated.[11]

This paper reports the synthesis and characterization of a new group of metal-containing dendrimers, namely, nanoparticle-cored dendrimers (NCDs). These dendrimers have gold nanoparticles at their core, and the dendrimers are generated by the self-assembly of disulfide-containing dendrimer wedges on the growing nanoparticle. Our strategy makes use of the Brust reaction, which was originally designed for the preparation of monolayer-protected clusters (MPCs) of Au atoms, as the final step in the dendrimer synthesis.[12] In the original Brust synthesis,

Scheme 1. Synthesis and Structure of NCD, Where G*n* Represents a Dendritic Wedge of Variable Generation Number

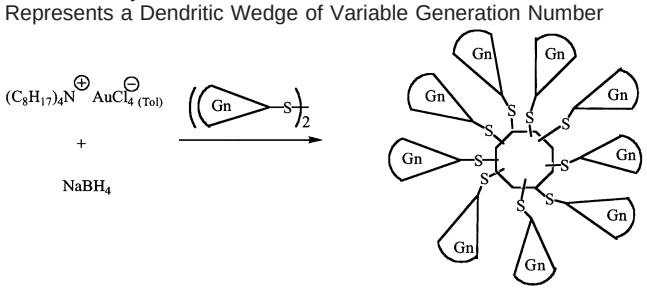

dodecanethiolate-protected gold clusters with a core diameter of 1−3 nm were prepared by the addition of aqueous sodium borohydride ($NaBH_4$) to a mixture of organic-phase-stabilized hydrogen tetrachloroaurate ($HAuCl_4$) and dodecanethiol. Subsequent reports have shown that a wide range of alkanethiolate chain lengths (C_3−C_{24}), ω-functionalized alkanethiolates, arenethiolates, and dialkylsulfides can be employed in the same protocol.[13] In this report, we demonstrate that reduction of $HAuCl_4$, phase-transferred into toluene using tetraoctylammonium bromide (TOAB), in the presence of Fréchet-type dendritic polyaryl ether wedges (G-1 to G-5) that have disulfide functionality, results in the formation of gold NCDs, as shown in Scheme 1.

This reaction is equivalent to the last step in a conventional convergent dendrimer synthesis, but there are a few obvious differences (vide infra). Similar to the alkanethiolate-coated MPCs, these NCDs are very stable in solution or as a solvent-free powder. They can be repeatedly dissolved in common organic solvents and recovered without decomposition or aggregation. Details regarding the synthesis and characterization of gold nanoparticle-cored polyaryl ether dendrimers of generation 1−5 are presented here.

Results and Discussion

Fréchet-type polyaryl ether dendritic wedges required for the synthesis of gold NCDs were prepared by reported procedures.[5a] The known dendritic bromides were converted to the thio derivatives by a procedure developed by Hu and Fox.[14] To force the reaction to completion, larger molar ratios of hexamethyl-

(6) (a) Fischer, M.; Vögtle, F. *Angew. Chem., Int. Ed*. **1999**, *38*, 884. (b) Frey, H.; Lach, C.; Lorenz, K. *Adv. Mater*. **1998**, *10*, 279. (c) Balzani, V.; Campagna, S.; Denti, G.; Juris, A.; Serroni, S.; Venturi, M. *Acc. Chem. Res*. **1998**, *31*, 26. (d) Zeng, F.; Zimmerman, S. C. *Chem. Rev*. **1997**, *97*, 1681.

(7) (a) Jian, D. L.; Aida, T. *J. Chem. Soc., Chem. Commun*. **1996**, 1523. (b) Enomoto, M.; Aida, T. *J. Am. Chem. Soc*. **1999**, *121*, 874. (c) Dandliker, P. J.; Diederich, F.; Gross, M.; Knobler, M.; Louati, A.; Sanford, E. M. *Angew. Chem., Int. Ed. Engl*. **1994**, *33*, 1739. (d) Bhyrappa, P.; Young, J. K.; Moore, J. S.; Suslick, K. S. *J. Am. Chem. Soc*. **1996**, *118*, 5708. (e) Pollak, K. W.; Leon, J. W.; Fréchet, J. M. J.; Maskus, M.; Abruna, H. D. *Chem. Mater*. **1998**, *10*, 30. (f) Newkome, G. R.; Guther, R.; Moorefield, C. N.; Cardullo, F.; Echegoyen, L.; Perezcordero, E.; Luftmann, H. *Angew. Chem., Int. Ed. Engl*. **1995**, *34*, 2023. (g) Chow, H. F.; Chan, I. Y. K.; Chan, D. T. W.; Kwok, R. W. M. *Chem.—Eur. J*. **1996**, *2*, 1085. (h) Gorman, C. B.; Smith, J. C.; Hagar, M. W.; Parkhurst, B. L.; Sierzputowska-Gracz, H.; Haney, C. A. *J. Am. Chem. Soc*. **1999**, *121*, 9958.

(8) (a) Newkome, G. R.; Cardullo, F.; Constable, E. C.; Moorefield, C. N.; Thompson, A. M. W. C. *J. Chem. Soc., Chem. Commun*. **1993**, 925. (b) Alonso, B.; Cuadrado, I.; Moran, M.; Losada, J. *J. Chem. Soc., Chem. Commun*. **1994**, 2575. (c) Takada, K.; Diaz, D. J.; Abruna, H. D.; Cuadrado, I.; Casado, C.; Alonso, B.; Moran, M.; Losada, J. *J. Am. Chem. Soc*. **1997**, *119*, 10763. (d) Kriesel, J. W.; Konig, S.; Freitas, M. A.; Marshall, A. G.; Leary, J. A.; Tilley, T. D. *J. Am. Chem. Soc*. **1998**, *120*, 12207. (e) Zhao, M.; Sun, L.; Crooks, R. M. *J. Am. Chem. Soc*. **1998**, *120*, 4877. (f) Balogh, L.; Tomalia, D. A. *J. Am. Chem. Soc*. **1998**, *120*, 7355. (g) Ottaviani, M. F.; Ghatlia, N. D.; Bossmann, S. H.; Barton, J. K.; Durr, H.; Turro, N. J. *J. Am. Chem. Soc*. **1992**, *114*, 8946. (h) Ottaviani, M. F.; Bossmann, S.; Turro, N. J.; Tomalia, D. A. *J. Am. Chem. Soc*. **1994**, *116*, 661.

(9) (a) Chechik, V.; Zhao, M.; Crooks, R. M. *J. Am. Chem. Soc*. **1999**, *121*, 4910. (b) Zhou, L.; Russel, D. H.; Zhao, M.; Crooks, R. M. *Macromolecules* **2001**, *34*, 3567. (c) Ottaviani, M. F.; Turro, N. J.; Jockusch, S.; Tomalia, D. A. *J. Phys. Chem*. **1996**, *100*, 13675. (d) Garcia, M. E.; Baker, L. A.; Crooks, R. M. *Anal. Chem*. **1999**, *71*, 256.

(10) (a) Crooks, R. M.; Zhao, M.; Sun, L.; Chechik, V.; Yeung, L. K. *Acc. Chem. Res*. **2001**, *34*, 181. (b) Zhao, M.; Crooks, R. M. *Chem. Mater*. **1999**, *11*, 3379. (c) Zhao, M.; Crooks, R. M. *Adv. Mater*. **1999**, *11*, 217.

(11) (a) Chechik, V.; Crooks, R. M. *J. Am. Chem. Soc*. **2000**, *122*, 1243. (b) Yeung, L. K.; Lee, C. T., Jr.; Johnston, K. P.; Crooks, R. M. *Chem. Commun*. **2001**, 2290. (c) Yeung, L. K.; Crooks, R. M. *Nano Lett*. **2001**, *1*, 14. (c) Rahim, E. H.; Kamounah, F. S.; Frederiksen, J.; Christensen, J. B. *Nano Lett*. **2001**, *1*, 499. (d) Niu, Y.; Yeung, L. K.; Crooks, R. M. *J. Am. Chem. Soc*. **2001**, *123*, 6840. (e) Zhao, M.; Crooks, R. M. *Angew. Chem., Int. Ed*. **1999**, *38*, 364. (f) Esumi, K.; Miyamoto, K.; Yoshimura, T. *J. Colloid Interface Sci*. **2002**, *254*, 402.

(12) Brust, M.; Walker, M.; Bethel, D.; Schiffrin, D. J.; Whyman, R. *J. Chem. Soc., Chem. Commun*. **1994**, 801.

(13) (a) Hostetler, M. J.; Green, S. J.; Stokes, J. J.; Murray, R. W. *J. Am. Chem. Soc*. **1996**, *118*, 4212. (b) Green, S. J.; Stokes, J. J.; Hostetler, M. J.; Pietron, J.; Murray, R. W. *J. Phys. Chem. B* **1997**, *101*, 2663. (c) Ingram, R. S.; Hostetler, M. J.; Murray, R. W. *J. Am. Chem. Soc*. **1997**, *119*, 9175. (d) Wuelfing, W. P.; Gross, S. M.; Miles, D. T.; Murray, R. W. *J. Am. Chem. Soc*. **1998**, *120*, 12696. (e) Hostetler, M. J.; Zhong, C.-J.; Yen, B. K. H.; Anderegg, J.; Gross, S. M.; Evans, N. D.; Porter, M.; Murray, R. W. *J. Am. Chem. Soc*. **1998**, *120*, 9396. (f) Templeton, A. C.; Hostetler, M. J.; Kraft, C. Y.; Murray, R. W. *J. Am. Chem. Soc*. **1998**, *120*, 1906. (g) Templeton, A. C.; Hostetler, M. J.; Warmoth, E. K.; Chen, S.; Hartshorn, C. M.; Krishnamurthy, V. M.; Forbes, M. D. E.; Murray, R. W. *J. Am. Chem. Soc*. **1998**, *120*, 4845. (h) Ingram, R. S.; Murray, R. W. *Langmuir* **1998**, *14*, 4115. (i) Green, S. J.; Pietron, J. J.; Stokes, J. J.; Hostetler, M. J.; Vu, H.; Wuelfing, W. P.; Murray, R. W. *Langmuir* **1998**, *14*, 5612. (j) Johnson, S. R.; Evans, S. D.; Brydson, R. *Langmuir* **1998**, *14*, 6639. (k) Porter, L. A.; Ji, D.; Westcott, S. L.; Graupe, M.; Czernuszewicz, R. S.; Halas, N. J.; Lee, T. R. *Langmuir* **1998**, *14*, 7378. (l) Chen, S.; Murray, R. W. *Langmuir* **1999**, *15*, 682. (m) Cliffel, D. E.; Zamborini, F. P.; Gross, S. M.; Murray, R. W. *Langmuir* **2000**, *16*, 9699. (n) Templeton, A. C.; Wuelfing, W. P.; Murray, R. W. *Acc. Chem. Res*. **2000**, *33*, 27. (o) Shon, Y.-S.; Gross, S. M.; Dawson, B.; Porter, M.; Murray, R. W. *Langmuir* **2000**, *16*, 6555. (p) Hu, J.; Zhang, J.; Liu, F.; Kittredge, K.; Whitesell, J. K.; Fox, M. A. *J. Am. Chem. Soc*. **2001**, *123*, 1464. (q) Zamborini, F. P.; Gross, S. M.; Murray, R. W. *Langmuir* **2001**, *17*, 481. (r) Fang, H.; Du, C.; Qu, S.; Li, Y.; Song, Y.; Li, H.; Liu, H.; Zhu, D. *Chem. Phys. Lett*. **2002**, *364*, 290. (s) Yang, W.; Chen, M.; Knoll, W.; Deng, H. *Langmuir* **2002**, *18*, 4124.

(14) Hu, J.; Fox, M. A. *J. Org. Chem*. **1999**, *64*, 4959.

Chart 1. Structures of Dendritic Sulfide Wedges Used in the Synthesis of NCDs

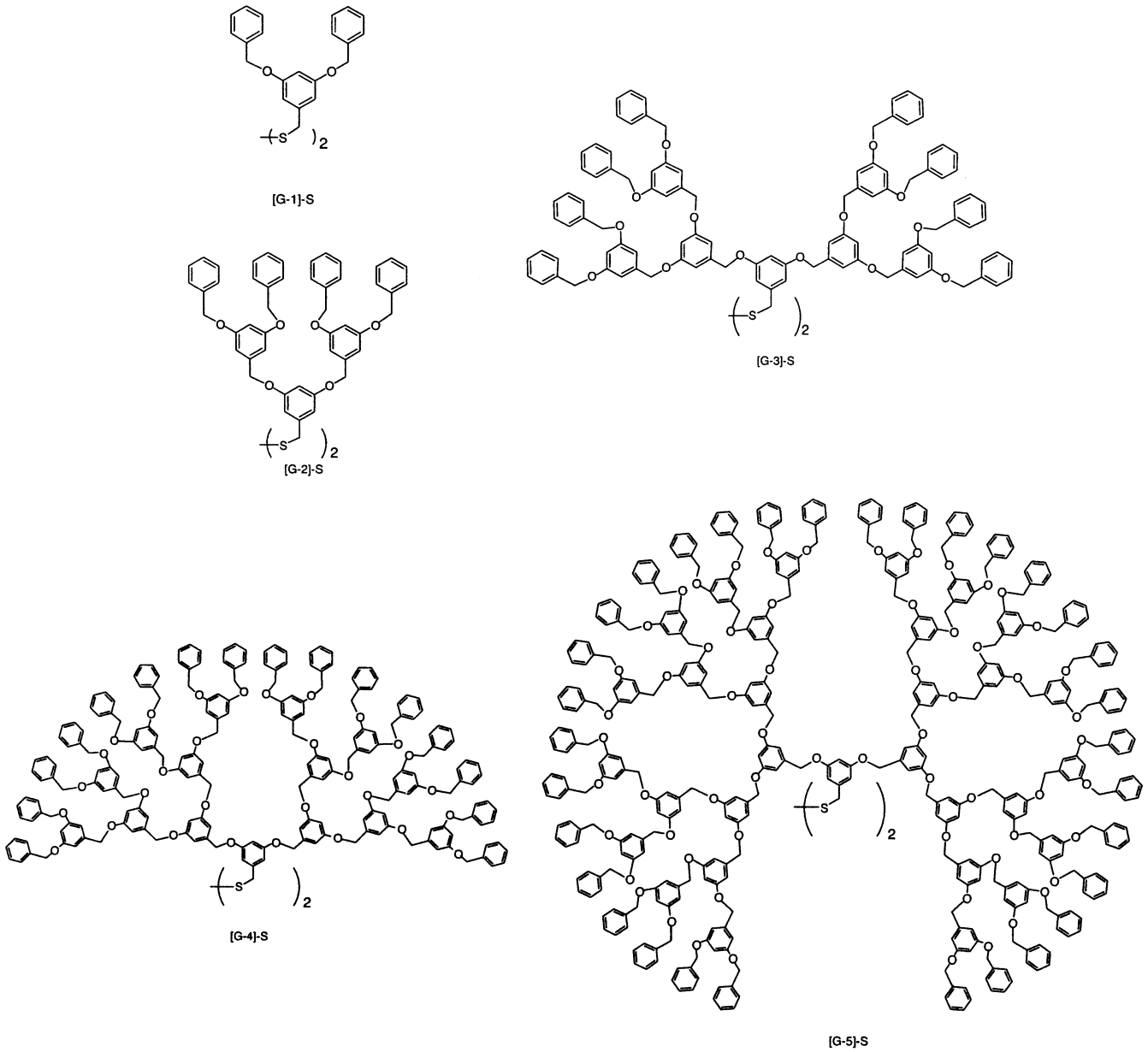

disilathiane and tetrabutylammonium fluoride and extended reaction times were used. This procedure resulted in the formation of disulfides from the initially formed thiols. These disulfides, designated as [G−*n*]-S, where *n* stands for the generation number of the dendritic wedge (Chart 1), were purified by column chromatography and characterized by the usual spectroscopic techniques. We observed that the dendritic disulfides occlude relatively large amounts of solvent molecules, such as the solvents used in their chromatographic purification. Rigorous purification with complete exclusion of the solvent was possible only in the cases of [G-1]-S and [G-2]-S. For the preparation of the gold NCDs described later in this paper, the disulfides were used without rigorous purification.

Gold NCDs were prepared by the Brust reaction. $HAuCl_4$ was phase-transferred into toluene using TOAB. The dendritic disulfide ([G-1]-S−[G-5]-S) dissolved in toluene was then added. The mixture was cooled briefly in ice and an excess of $NaBH_4$ was added. The resulting black solution was stirred for 2 days at room temperature. We did not observe the precipitation or formation of insoluble materials during any of these preparations. The toluene layer was then separated and the gold NCDs were isolated, using the standard protocol described in the Experimental Section. In the following sections, these NCDs are referenced as Au−G-*n*, where *n* corresponds to the generation number of the polyaryl ether dendritic wedge.

It is well-known that the size distribution of gold nanoparticles produced by the Brust synthesis depends on factors such as reaction temperature, gold/thiol molar ratio, and rate of addition of reductant, and it is generally customary to conduct the synthesis at different gold/thiol molar ratios, to study the properties of the resulting clusters.[13,15] In the present case, the limited amount of available synthetic, fully purified segments

(15) Hostetler, M. J.; Wingate, J. E.; Zhong, C.-J.; Harris, J. E.; Vachet, R. W.; Clark, M. R.; Londono, J. D.; Green, S. J.; Stokes, J. J.; Wignal, G. D.; Glish, G. L.; Porter, M. D.; Evans, N. D.; Murray, R. W. *Langmuir* **1998**, *14*, 17.

made it impossible to explore the entire range of conditions for the preparation of these composites. For example, dendritic disulfides [G-4]-S and [G-5]-S were prepared at the end of 10 and 12 reaction steps, respectively, and these were not available for several reactions under different conditions. Hence, we have used one set of conditions for the preparation of all the NCDs described here. The reproducibility of the synthesis, however, was ascertained by repeating the reactions twice with [G-4]-S and [G-5]-S and three times with other dendritic disulfides.

The NCDs thus prepared were black powders, freely soluble in methylene chloride, chloroform, toluene, and tetrahydrofuran (THF). Dilute solutions of Au−G-1, Au−G-2, and Au−G-3 were brown in color (cola-colored), whereas those of Au−G-4 and Au−G-5 appeared pink. These are very stable in solution and in solvent-free forms. Solutions of Au−G-*n* in methylene chloride were observed for more than four months, and no decomposition or precipitation was noted in any of the cases. All the NCDs were insoluble in methanol, ethanol, and diethyl ether. The NCDs incorporate substantial amounts of toluene and TOAB (used as the phase-transfer agent in the Brust reaction). Unsuccessful attempts were made to remove these by Soxhlet extraction using ethanol as the solvent and by precipitation from THF into ethanol. Even after performing the extraction for a week, some TOAB (∼5%) still remained trapped inside the NCDs. The NCDs did not exhibit any decomposition during the Soxhlet extraction procedure. Furthermore, attempts at NCD precipitation from a variety of mixed solvents proved futile.

The Brust reaction was performed using the dendritic bromide wedges [G-1]-Br−[G-5]-Br, instead of the disulfides, and these served as control experiments. In the case of [G-1]-Br−[G-4]-Br, the reactions yielded black particles, which resembled the nanoparticles obtained in the disulfide reactions. Solutions of these nanoparticles, however, were not stable. Within 5−10 min of dissolution in a solvent such as chloroform, black particles settled at the bottom, leaving a clear, colorless supernatant liquid. ^{1}H NMR spectra of the supernatant solutions showed the presence of TOAB and dendritic wedges. For the [G-1]-Br−[G-3]-Br cases, the peak at $\delta \approx 4.3$ due to the CH_2Br group disappeared and a new peak appeared at $\delta = 2.83$. We believe that the CH_2Br groups in these dendritic wedges were converted to CH_3 groups under the reaction conditions. These solutions were not analyzed in any further detail. In the case of the control experiment with [G-5]-Br, the solution became black immediately after the addition of $NaBH_4$, but overnight stirring resulted in the formation of small, yellow gold beads.

The formation of unstable nanoparticles in the control experiments sheds some light on the actual course of the reaction. For the larger dendritic disulfides, the sulfide group is a very small functionality and these groups are expected to react slowly with the growing gold nanoparticles. Competitive formation of very large gold clusters and even precipitation of gold particles were, in fact, anticipated in the reactions. Surprisingly, no trace of any insoluble material was seen in any of these preparations. We believe that encapsulation of the growing gold clusters within the cavities of the dendritic disulfides plays a significant role. Small gold clusters are initially formed within a TOAB cavity and soon migrate into cavities provided by the dendritic wedges. The trapped cluster eventually finds a disulfide group and reacts with it in a very slow process. In this respect, the disulfides may function better than the corresponding thiols, for two reasons. First, there are two dendritic wedges in a disulfide, and they may provide better cavities for encapsulation. Second, after the gold cluster finds a disulfide group, two Au−S bonds can be formed at the same time, resulting in the formation of a stable, well-protected NCD. In the case of the control experiments with dendritic bromide wedges, the initially formed clusters, along with the TOAB molecules, are protected to some extent by the dendritic wedges. The workup involves removal of toluene and repeated sonication of the residue with ethanol. This procedure removes most of the TOAB molecules. When the nanoparticles are redissolved in a solvent, they agglomerate and precipitate within a short period of time. In the case of [G-5]-Br, the formation of gold beads suggests that the initially formed nanoparticles fail to penetrate into the dendritic wedges. This may be a result of increased steric congestion arising from the dense packing of surface groups in the [G-5] dendritic bromide.

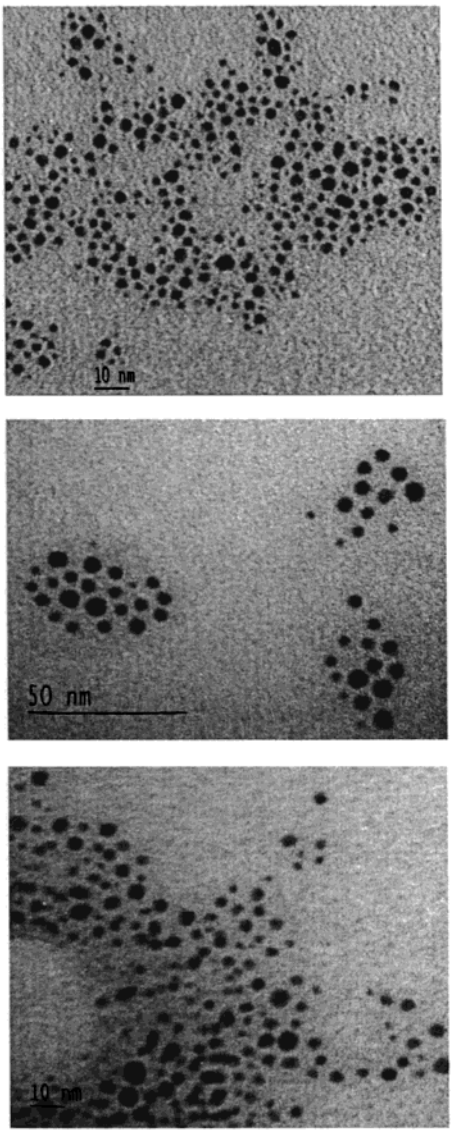

Figure 1. TEM images for (top) Au−G-1, (middle) Au−G-4, and (bottom) Au−G-5.

It is widely known that the Brust synthesis of MPC involves three steps, namely nucleation, growth, and passivation.[13] Our

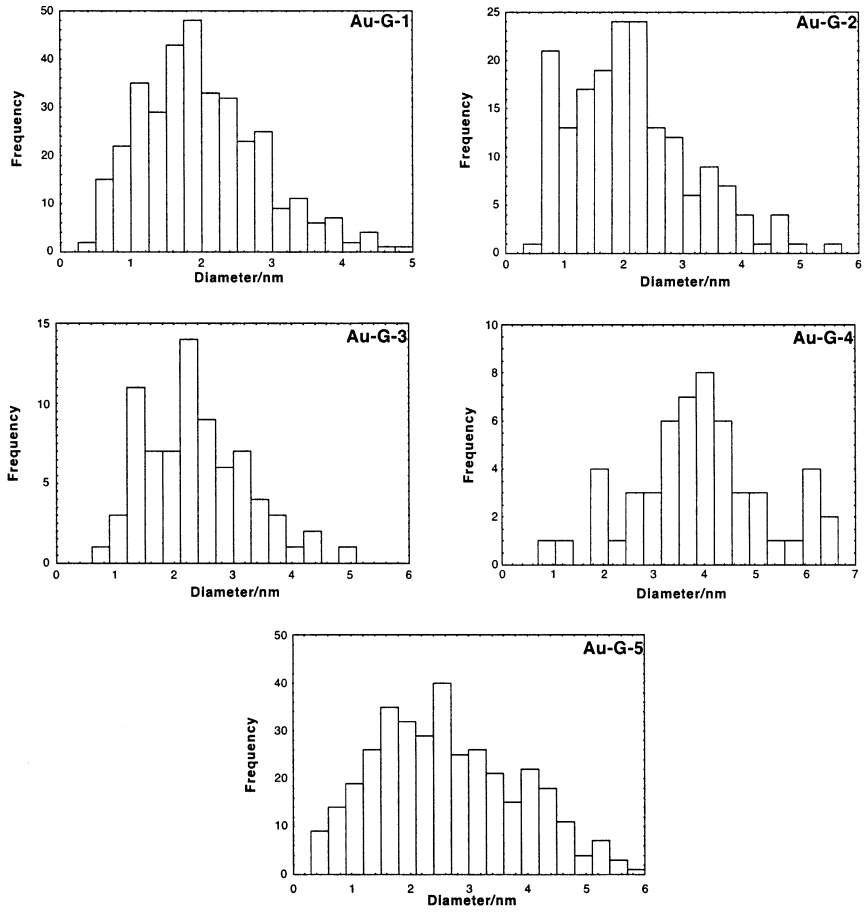

Figure 2. Core-size histograms for Au-NCDs.

Table 1. TEM, TGA, and Absorption Spectral Data for Au-NCDs

Au–NCD	average core diameter (nm)	content (wt %) Au	content (wt %) [G-*n*]-S[a]	surface plasmon λ_{max} (nm)
Au−G-1	2.01	88.15	11.85	491
Au−G-2	2.13	67.80	27.20	496
Au−G-3	2.37	58.87	36.13	522
Au−G-4	3.93	66.69	28.31	528
Au−G-5	2.62	70.11	24.89	524

[a] Corrected for adsorbed TOAB.

observations suggest that the formation of NCDs may involve one additional step: nucleation, growth, encapsulation, and passivation.

Characterization of NCDs. The NCDs of generations G-1 to G-5 were analyzed by high-resolution transmission electron microscopy (HRTEM), thermogravimetric analysis (TGA), and UV, IR, and NMR spectroscopies.

Transmission Electron Microscopy. HRTEM has provided extensive information about the size and, to a much lesser extent, the shapes of metal nanoparticles.[13] Figure 1 gives the HRTEM images of Au−G-1, Au−G-4, and Au−G-5. Core-size histograms of Au−G-1−Au−G-5 are shown in Figure 2. These figures show that the NCDs are relatively small and do not possess a uniform core size. The core sizes exhibit a relatively wide distribution. The linear average diameters of the populations of nanoparticles are given in Table 1. The average core size increases from Au−G-1 to Au−G-4 and then shows a decrease as the dendron wedge size increases to Au−G-5. It is well-known that the core sizes of MPCs depend very sensitively on reaction conditions.[15] Although we have used only one set of reaction conditions, it is expected that entirely different size distribution patterns would result under other reaction conditions. Here, we emphasize that the distribution of core diameters of NCDs is comparable to that of MPCs prepared under similar conditions.

HRTEM images only the Au core, and the core−core separation distance is generally taken as the length of the alkyl chain in alkanethiolate MPCs. In the present case, occurrences of relatively identical core−core separations were rare in the TEM images and, hence, the thickness of the dendritic layer could not be estimated from the images. It has been suggested that the cores in Au-MPCs have icosohedral or cuboctahedral shapes. However, TEM analysis of fractionally crystallized MPCs, combined with matrix-assisted laser desorption ionization (MALDI) mass spectra and theoretical calculations, has determined that a more likely shape of the Au core in MPCs is a truncated octahedron.[15] From the HRTEM images of Au-NCDs (Figure 1), one cannot make any conclusion about the shapes of these particles. They appear approximately spherical, and the situation is comparable to several reported cases of Au-MPCs.[13]

Thermogravimetric Analysis. It has been shown that the progressive heating of MPCs leads to volatilization of the organic fraction as disulfides, leaving a residue of gold. TGA is therefore the preferred technique to estimate the total organic content of the MPC.[13,16] We have performed TGA studies on Au−G-1−Au−G-5 (Figure 3). Values of the weight percentages of gold obtained from the thermograms are collected in Table 1.

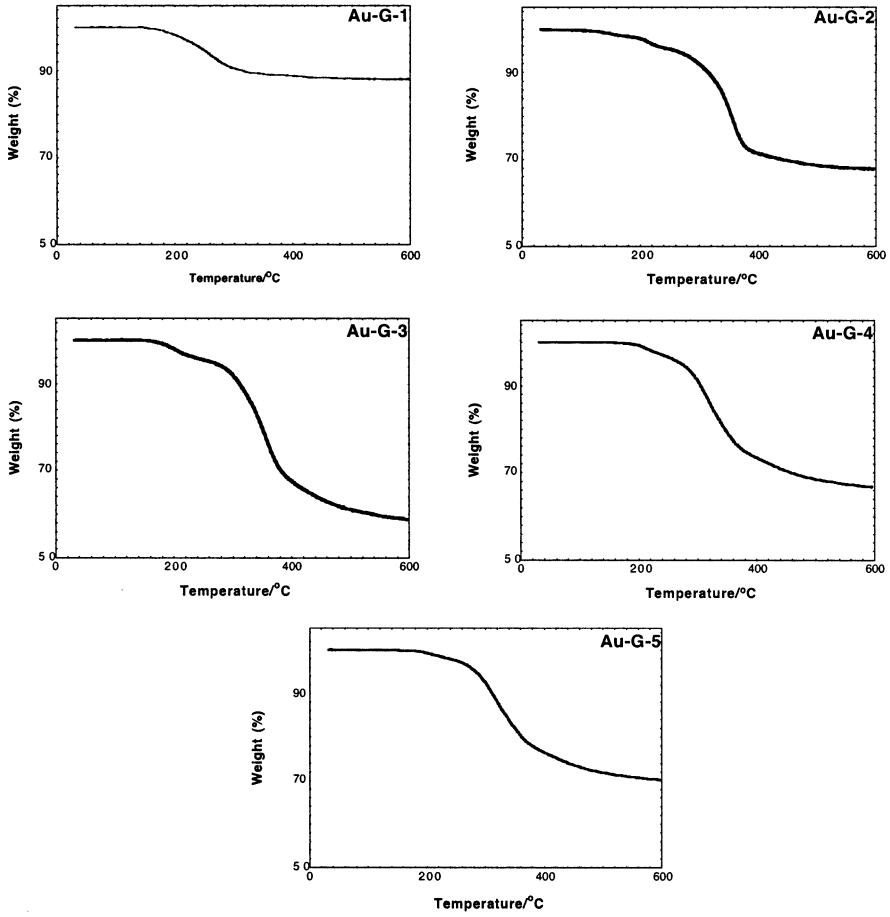

Figure 3. Thermograms for Au-NCDs. Temperature increment was 10 °C/min.

For C_8-, C_{12}-, and C_{16}-coated MPCs, thermal decomposition occurred in a single, well-defined step ~100 °C wide, beginning at 230, 266, and 310 °C, respectively.[16] The NCDs present a slightly different case. For Au−G-1, the total organic content was ~12% and volatilization occurred in a single step starting at 150 °C. For the other NCD generations, the volatilization process occurred in two stages. The first stage, which contributes to ~5% of the weight loss, is attributed to the removal of trapped solvent and TOAB. ^{1}H NMR spectrum of Au−G-1 shows very little TOAB, and, in this case, the organic fraction consists mostly of the dendritic sulfide. For the higher-generation NCDs, the second decomposition step started at temperatures above 200 °C, indicating thermal stabilities that are comparable to those of alkanethiolate MPCs.[15] The percentage weights of dendritic wedges in these NCDs are also presented in Table 1. Notice that, for Au−G-1, this number is equal to 100% Au, but for other generations of Au-NCD, this fraction is equal to 100% Au − (5% contribution due to TOAB).

Absorption Spectroscopy. Ultraviolet−visible (UV−vis) spectroscopy is a very useful technique for the characterization of nanoparticles.[13,17] The absorption spectra of Au−G-1−Au−G-5 in dichloromethane solution are shown in Figure 4. The absorption spectra exhibit a smoothly increasing absorption at increasing energy (so-called Mie scattering), with a superimposed surface plasmon band between 450 and 600 nm. The plasmon band is responsible for the colors exhibited by the nanoparticles, and it arises from interband transitions between the highly polarizable Au 5d[10] band and the unoccupied states of the conduction band.[17] The plasmon bands of Au−G-1 and Au−G-2 look similar. The first derivative spectra put the plasmon absorption maxima at 491 and 496 nm, respectively, for these NCDs. The plasmon band maxima for the other NCDs occurred at ~520 nm, and all these values are collected in Table 1. A comparison with the TEM data suggests that the plasmon band maxima show a dependence on particle size. The plasmon band maxima for these NCDs are similar to those for arenethiolate-capped MPCs reported in the literature.[13]

According to Mie theory, approximated to include only the first term in the electric dipole expansion appropriate for particle diameters <30 nm, the extinction coefficient per particle is proportional to the particle volume.[17a] Thus, the intensity of the plasmon band is expected to increase with the average particle size of the nanoparticles. A visual inspection of Figure 3 suggests that the intensities of the plasmon bands are in the following order: Au−G-1 ≈ Au−G-2 < Au−G-3 < Au−G-5 < Au−G-4. This is in accordance with the data obtained by TEM. The plasmon band maxima and intensity did not exhibit any solvent dependence, because the spectra obtained in THF exhibited the same features observed in dichloromethane for all the NCD generations.

(16) Terril, R. H.; Postlethwaite, T. A.; Chen, C.-H.; Poon, C.-D.; Terzis, A.; Chen, A.; Hutchison, J. E.; Clark, M. R.; Wignall, G.; London, J. D.; Superfine, R.; Falvo, M.; Johnson, C. S., Jr.; Samulski, E. T.; Murray, R. W. *J. Am. Chem. Soc.* **1995**, *117*, 12537.

(17) (a) Duff, D. G.; Baiker, A.; Edwards, P. P. *Langmuir* **1993**, *9*, 2301. (b) Wilcoxon, J. P.; Martino, A.; Baughmann, R. L.; Klavetter, E.; Sylwester, A. P. *Mater. Res. Soc. Symp. Proc.* **1993**, *286*, 131. (c) Kreibig, U.; Genzel, L. *Surf. Sci.* **1985**, *156*, 678.

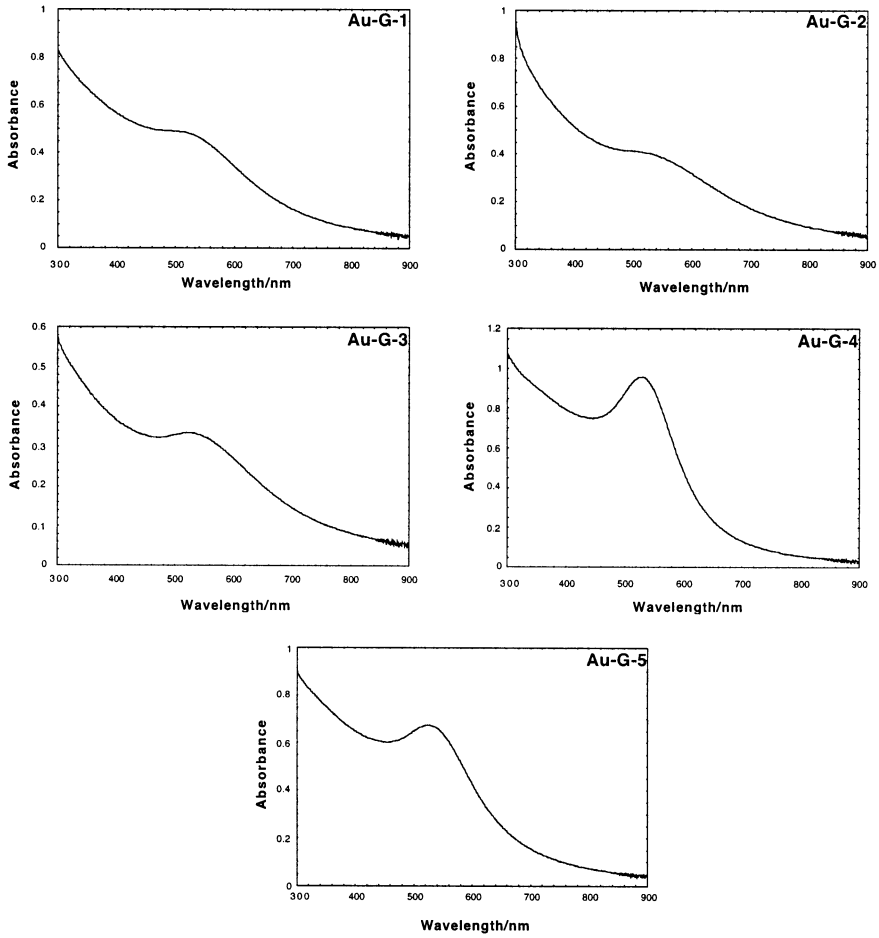

Figure 4. UV−vis spectra of Au-NCDs in dichloromethane. [Au−G-*n*] ≈ 1 mg/10 mL.

FTIR Spectra. For the alkanethiolate-protected MPCs, IR spectroscopy has provided valuable information regarding the conformation and ordering of the alkyl chains on the metal surface.[13,18] The frequency and bandwidth in the C−H and C−C stretching regions, in particular, are indicative of order in the MPC. In the case of arenethiolate MPCs, IR spectra were less useful.[13l] This is also the case for NCDs. IR spectra of the dendritic disulfides and the Au-NCDs were very similar. For example, Figure 5 shows the FTIR spectra of Au−G-4 and the G-4 disulfide. The only discernible difference in these spectra is the increase in intensity of the band in the 2900−2800 cm^{-1} region. This band, which arises due to C−H stretching vibrations, is attributed to the CH_2 groups in TOAB, which is present as an impurity (∼5%) in the NCD. Except for this small difference, the IR spectra of all the Au-NCDs and dendritic sulfides [G−*n*]-S were almost identical.

NMR Spectra. The organic content in Au−G-1 is very small; hence, ^{13}C NMR of this NCD could not be obtained. ^1H and ^{13}C NMR spectra of all the other NCDs were obtained in $CDCl_3$ solution. For the fourth- and fifth-generation NCDs, the ^1H and ^{13}C NMR signals of the CH_2−S group were very weak or nonobservable. The ^1H NMR and ^{13}C NMR spectra of the second-generation dendritic wedge ([G-2]-S) and the corresponding NCD are compared in Figures 6 (^1H NMR) and 7 (^{13}C NMR). In the ^1H NMR spectra, the peaks at δ 1.56 are due to the residual water present in the $CDCl_3$. For Au−G-2, the small hump at approximately δ 2.8 and the peaks below δ 1.6 are attributable to the residual TOAB present as a trapped impurity within the NCD. The peaks due to TOAB can also be seen in the ^{13}C NMR spectrum of Au−G-2 (Figure 7). The ^{13}C NMR spectrum of [G-2]-S was almost identical to that of Au−G-2, except for the presence of the small signals due to TOAB. In the ^1H NMR spectra, the peak due to CH_2−S at δ 3.55 appears very similar for [G-2]-S and Au−G-2. The bases of the other peaks in Au−G-2 are broadened significantly. This broadening was also present in the ^1H NMR spectra of all the NCD generations; the reason for this broadening is unclear at this time. Because of this broadening, the integrations for the proton signals were not very accurate.

For the alkanethiolate-protected gold MPCs, the ^1H and ^{13}C NMR signals were characteristically broadened, relative to those of free alkanethiols.[13] In fact, the NMR line widths in MPCs varied systematically with the position of the carbon site, relative to the Au core. Several reasons have been put forth to explain the NMR line broadening in MPCs.[13,19] Most important among these is the solidlike packing of the methylene chains closest to the Au core. Near the Au core, the methylene chains experience restricted motion, whereas those far removed from the core experience freedom of movement as in a liquid, leading to a broadening of NMR signals for groups near the core and relatively little or no broadening of signals for groups far removed from the core. Line broadening can also be due to the

(18) Hostetler, M. J.; Stokes, J. J.; Murray, R. W. *Langmuir* **1996**, *12*, 3604.

(19) Badia, A.; Lennox, R. B.; Reven, L. *Acc. Chem. Res.* **2000**, *33*, 475.

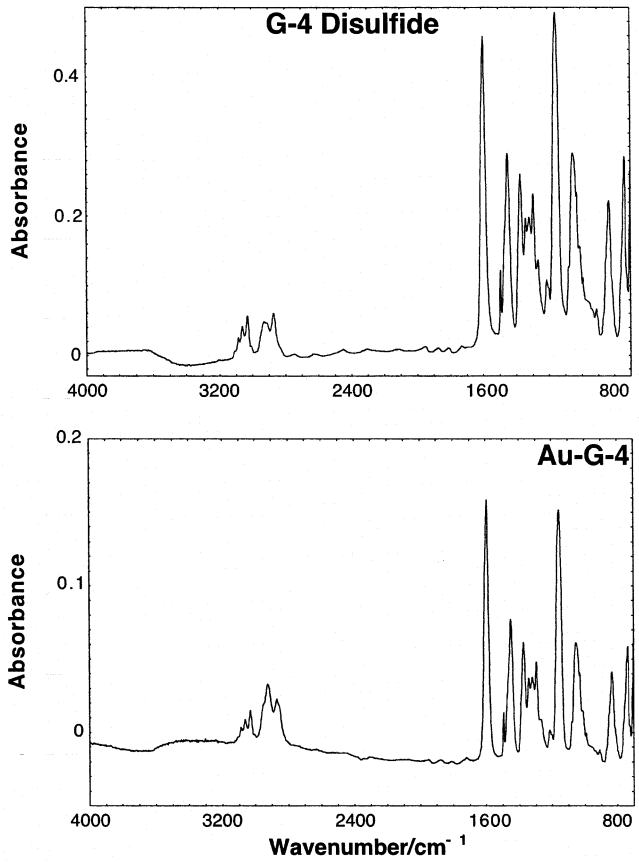

Figure 5. FT-IR absorbance spectra of [G-4]-S and Au−G-4.

existence of a distribution of chemical shifts caused by the differences in the Au−S binding sites (terraces, edges, vertices) or due to spin−spin relaxation (T_2-broadening).[15]

If the NMR line broadening in MPCs is due to solidlike packing near the metal core, one can predict that such an effect will be absent in NCDs. In a typical NCD (Scheme 1), the methylene groups attached to the S atoms do not experience any steric crowding. In contrast, when several dendritic wedges self-assemble on the Au nanoparticle core (Scheme 1), they enclose large void spaces near the core. The CH_2−S groups attached to the core experience relatively little or no crowding and steric congestion increases as one proceeds toward the exterior of the NCD. The situation is analogous to the De Gennes dense packing in dendrimers.[20] Thus, if NMR line broadening were to occur in NCDs because of steric crowding, it should be associated with the NMR signals of the outermost groups and in the reverse order of that seen in MPCs. In fact, for all NCD generations, the ^{1}H NMR signals of the outer phenyl groups are broadened at the base, but it is not clear if this is due to dense packing. Most probably, this broadening is not due to dense packing, because no broadening was observed for ^{13}C signals in any of the Au-NCD generations.

NaCN-Induced Decomposition of NCDs. Earlier work on alkanethiolate/gold two-dimensional (2D) self-assembled monolayers (SAMs)[21] and alkanethiolate MPCs[13f,l] have shown that cyanide causes dissociation of the monolayer with concomitant

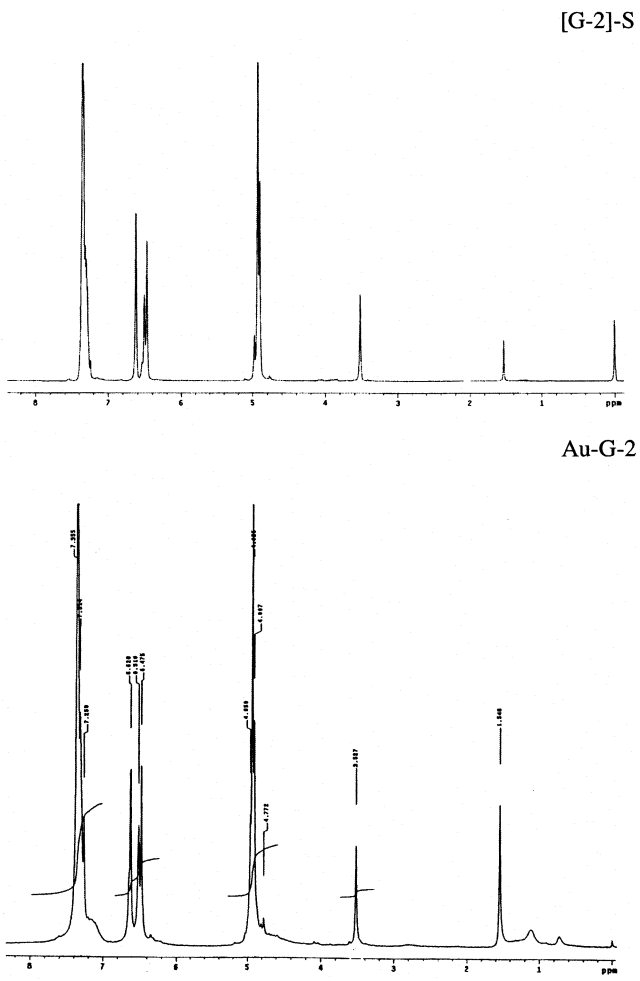

Figure 6. ^{1}H NMR spectra of [G-2]-S and Au−G-2 in $CDCl_3$.

etching or dissolution of the gold. The cyanide must penetrate the protective organic layer for it to react with the gold. The rate of decomposition of the SAM or MPC by NaCN can, therefore, be correlated to the extent of protection that the organic layer provides to the gold surface. To see if the dendritic layers provide good protection to the Au core, we have performed the cyanide-induced decomposition of Au−G-1−Au−G-5 under pseudo-first-order conditions (an excess of cyanide).

Our experiments show that the dark-brown or pink Au-NCD solutions are converted to a colorless solution by NaCN in 6:1 THF/H_2O. The decomposition reactions were followed by UV−vis spectroscopy. Figure 8 shows the changes in absorption as a function of time for the various generations of NCDs at 520 nm, following the addition of NaCN. The decay data were fit to a general first-order equation: $y = y_0 + a \exp(-kt)$, where y is the experimental absorbance and y_0 is a constant term accounting for the small amount of residual absorption.[13f,l] Fits of the data to this equation were very bad for all NCD generations (correlation < 0.9). Subsequently, the data were fit to a two-exponential function: $y = y_0 + a \exp(-k_1t) + b \exp(-k_2t)$. Fits of the data to this equation were very good for all Au-NCDs (correlation > 0.99). For Au−G-1 (Figure 8, top panel), the fit is shown superimposed on the experimental decay curve; the curves are indistinguishable from each other. The

(20) De Gennes, P. G.; Hervet, H. J. *J. Phys. Lett. (Paris)* **1983**, *44*, 351.
(21) (a) Kumar, A.; Whitesides, G. M. *Appl. Phys. Lett.* **1993**, *63*, 2002. (b) Weisbecker, C. S.; Merritt, M. V.; Whitesides, G. M. *Langmuir* **1996**, *12*, 3763. (c) Gorman, C. B.; Biebuyck, H. A.; Whitesides, G. M. *Chem. Mater.* **1995**, *7*, 252.

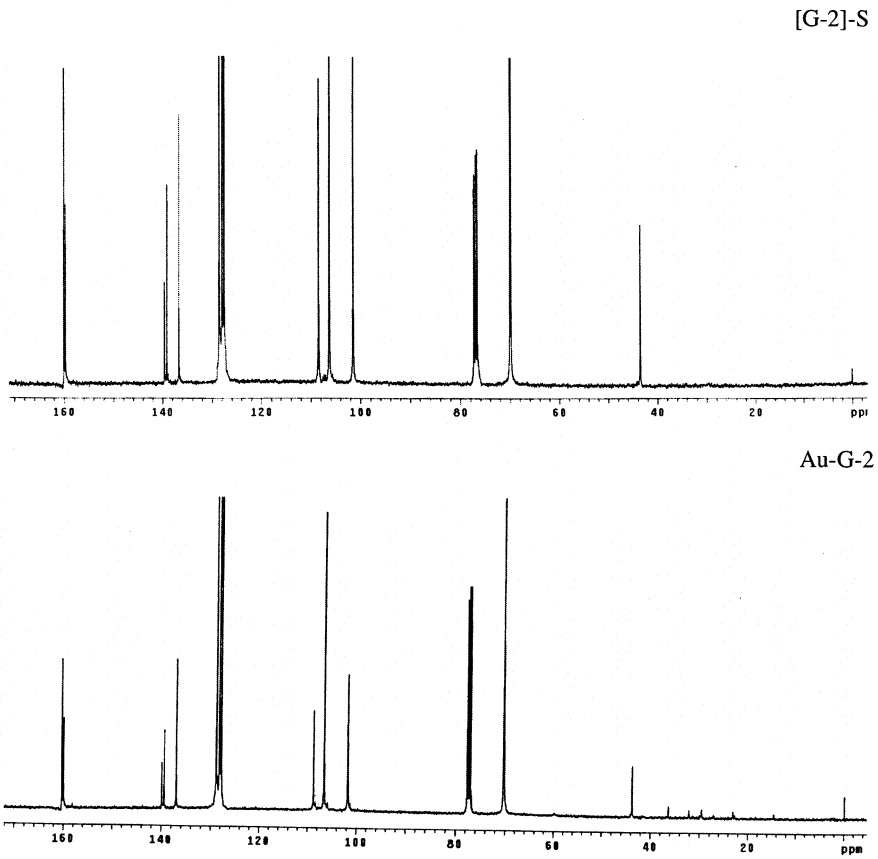

Figure 7. ^{13}C NMR spectra of [G-2]-S and Au−G-2 in $CDCl_3$.

fits were of similar quality for all the NCDs generations. Values of k_1 and k_2 obtained for the various NCDs are presented in Table 2.

Cyanide-induced absorption changes for MPCs follow the single-exponential equation, and decomposition is most rapid for clusters protected by short alkyl chains and slowest for longer alkyl chains.[13f,l] This is consistent with the concept that longer alkyl chains give better protection to the Au core at the center. A different trend is observed in the case of Au-NCDs. Cyanide-induced decomposition of Au−G-1 was very slow. In fact, decomposition in this case was much slower than most cases of MPC decomposition reported in the literature. For other generations of NCDs (Figure 8, bottom panel), decomposition occurred in a time scale comparable to that of alkanethiolate and arenethiolate MPCs.[13f,l]

The occurrence of two decomposition rate constants is not well understood. We tentatively attribute this to the presence of two types of NCDs in each generation, one which has its surface relatively well covered by the dendrimer wedges and a second type, which is relatively open. The values of k_1 increased from Au−G-1 to Au−G-5, but those of k_2 increased from Au−G-1 to Au−G-4 and decreased for Au−G-5. Considering only k_1, we conclude that the accessibility of the core increases with generation number.

General Comments Regarding the Structure of NCDs. Results from the TEM and TGA studies can be combined to get useful information regarding the structure of the NCDs. From the TEM size distributions, one can obtain the average diameter of the nanoparticles (Table 1). This value can be used to extract the approximate number of Au atoms in the cluster using the density (59 atoms/nm^3) of bulk face-centered cubic (fcc) gold. The approximate number of Au atoms in a cluster is given by the relation $N_{Au} = (59 \text{ atoms/nm}^3)(\pi/6)D^3$, where D is the average diameter of the nanoparticle (in nanometers).[13s] The weight of the gold core is given by $N_{Au} \times 197$ (where 197 is the atomic weight of gold). This weight is equated to the weight percentage of gold from the TGA experiments, to obtain the average total weight of the NCD. The percentage weight of the dendritic fraction is known (Table 1); therefore, we can calculate the total weight of the dendritic fraction in the NCD. This value is divided by the molecular weight of the dendritic thio unit to obtain the average number of dendrimer units present on the nanoparticle core in each of the NCD generations. In Table 3, we have provided the calculated values of N_{Au}, the weight of the gold core, the weight of the dendritic fraction, and the average number of dendritic wedges (rounded to the nearest integer) for all the NCD generations. Attempts to confirm these molecular weights by matrix-assisted laser desorption ionization−time-of-flight (MALDI−TOF) experiments were not successful.

If all the NCDs have perfectly spherical cores of equal diameter, one can expect that the number of dendritic wedges present will decrease as the generation number increases. The diameters of the NCDs are not the same and details about their shapes are not known, thus making a direct comparison difficult. A better approach would be to compare the number of dendritic wedges attached to the unit surface area of the Au core. We have calculated this value (Table 3), assuming that the particles are spherical. It can be seen from Table 3 that the number of dendritic wedges per square namometer decreases steadily for

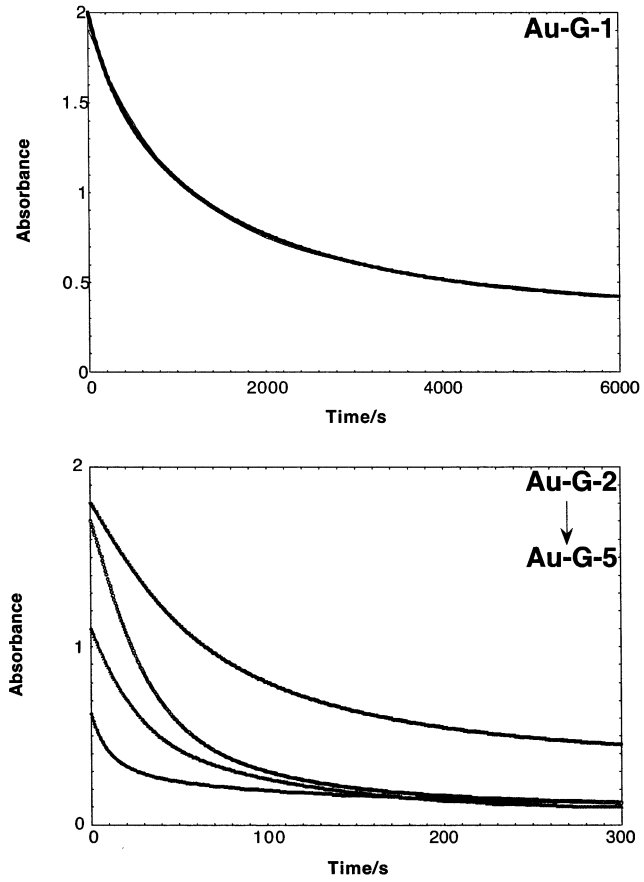

Figure 8. NaCN-induced decomposition of Au−G-*n*. Absorbance changes were followed at 520 nm.

Table 2. Rate Constants for the Decomposition of Au−NCDs with NaCN

Au–NCD	k_1, s^{-1}	k_2, s^{-1}
Au−G-1	$(1.29 \pm 0.01) \times 10^{-3}$	$(2.25 \pm 0.15) \times 10^{-4}$
Au−G-2	$(1.67 \pm 0.003) \times 10^{-2}$	$(2.88 \pm 0.01) \times 10^{-3}$
Au−G-3	$(3.21 \pm 0.007) \times 10^{-2}$	$(7.56 \pm 0.04) \times 10^{-3}$
Au−G-4	$(4.46 \pm 0.02) \times 10^{-2}$	$(1.10 \pm 0.003) \times 10^{-2}$
Au−G-5	$(6.49 \pm 0.04) \times 10^{-2}$	$(4.03 \pm 0.002) \times 10^{-3}$

Au−G-2 to Au−G-5; Au−G-1 is an exception. For all cases of NCDs, the occupancy per square namometer is much lower than that reported for alkanethiolate- (4.7/nm^2) and arenethiolate-protected (5−9/nm^2) MPCs.[13l]

Our experiments have not provided direct evidence for the presence of Au−S bonds in the NCDs, and one might argue that the gold clusters may be present as trapped materials and not as structural units of the dendrimer. However, several arguments can be presented against this possibility. First, we have only dendritic wedges—no dendrimers—in the reaction mixture. Dendritic wedges, particularly the lower-generation ones, typically do not possess encapsulation properties. Except perhaps for the Au−G-5 case, the Au cores are larger than the dendritic wedges and, thus, encapsulation is not physically possible. Examples of nanoparticles encapsulated in PAMAM dendrimers (G ≥ 4) are available in the literature.[10,11] The diameter of the 4G PAMAM dendrimer is 4 nm, which is much larger than the nanoparticle and several times bigger than the Fréchet-type dendritic wedges used in this study. A model wherein several dendritic wedges assemble together and provide a cavity for encapsulation of the nanoparticle can also be considered. This model, however, is not supported by the model experiments with dendritic bromides. Decomposition studies with cyanide also do not support the encapsulation model. If the gold particles are protected by encapsulation, then protection should be greater for larger dendrimer wedges, which is not observed experimentally. Finally, encapsulated particles should aggregate and precipitate after some time. We observed the solutions of the NCDs for more than four months and no changes were noted.

It is imperative at this point to compare the NCDs to conventional dendrimers prepared by the convergent approach. There are several differences. In the conventional convergent synthesis of dendrimers, the number of covalent bonds formed in the final step is known and, therefore, the molecular weight is precisely known. In the NCD synthesis, the last step is a self-assembly process and is controlled by the availability of surface space and ligands. Hence, a distribution of molecular weights can be anticipated. In a convergent synthesis, the number of dendritic wedges reacting in the final step rarely exceeds four. The number of wedges reacting can be very high in NCDs (Table 3), and the reaction conditions can be manipulated to vary this number.

Another significant difference is the shape and morphology of the dendritic architecture. In conventional dendrimers, the lower-generation (G < 3) members are open structures and do not possess the so-called "dendritic properties". Dendrimers assume a globular shape at G ≥ 3. In the case of NCDs, assembly of the dendritic wedges is on an almost-spherical 3D core, and, hence, the first generation itself can have dendritic properties. In the case of conventional dendrimers, the core becomes less accessible as the generation number increases. In the case of the NCDs, cyanide decomposition experiments showed that the CN group reaches the core faster for the higher generations. This is mostly due to irregularities in the assembling of the wedges. The smaller wedges can pack better on the surface, leading to uniform surface coverage and, thus, a reduction in core reactivity. As the size of the wedge increases, the spatial requirement of the branch increases and the packing becomes less efficient, exposing the core to approaching reagents. This aspect may have significant implications in the use of NCDs as catalysts in organic reactions.

A comparison of NCDs with MPCs is also imperative. In the MPCs, packing of the ligands is assumed to be uniform. The methylene groups are closely packed near the core but are free to move at the periphery. We expect the opposite situation in NCDs. NCDs can be considered as MPCs with dendritic properties. The wedges in NCDs may enclose large void spaces in the interior and, depending on the generation number, the surface may have irregularities. Compared to the MPCs, the NCDs have very few ligands. Thus, a large fraction of the surface of the metal core is unpassivated. This may have important implications for the use of these materials as catalysts.

Transition-metal nanoparticles are of great technological importance, because of their applications to catalysis.[22] Metal nanoparticles for catalysis are usually prepared by evaporation/

(22) (a) *Clusters and Colloids*; Schmidt, G. Ed.; VCH: Weinheim, Germany, 1994. (b) *Colloidal Gold: Principles, Methods and Applications*; Academic Press: San Diego, CA, 1991. (c) *Metal Nanoparticles: Synthesis, Characterization and Applications*; Feldheim, D. L., Foss, C. A., Jr., Eds.; Marcel Dekker: New York, 2002.

Table 3. Calculated NCD Parameters

Au–NCD	no. of core Au atoms	weight of Au core[a]	weight of dendritic fraction[a]	molecular weight of Ar–S unit[a]	no. of wedges per particle	no. of dendritic wedges per nm^2
Au−G-1	251	49447	6254.50	335	20	1.58
Au−G-2	298	58706	23551.66	759	31	2.18
Au−G-3	411	80967	49691.48	1607	31	1.76
Au−G-4	1874	369178	156716.58	3303	47	0.97
Au−G-5	555	109335	38815.40	6695	6	0.27

[a] Atomic and molecular weights given in daltons.

condensation of the metal or by electrochemical/chemical reduction of metal salts. Stabilizers such as polymers, ligands, or surfactants are used in these preparations to control particle size and prevent agglomeration. This process, however, leads to partial passivation of the catalyst surface and, thus, reduced catalytic activity. Hence, there is a need for new nanoparticle technologies that provide the highest protection and the least passivation.

NCDs fit this scheme very well. Table 3 shows that Au−G-5, which is indefinitely stable, has only six dendritic wedges attached to the core. Because of the dendritic architecture, NCDs enclose large void spaces near the core. Thus, most of the metal core in NCDs is available for catalysis. In addition, the dendritic layer can exhibit container/scaffolding properties, helping to bring the reactants to the metal core. Several dendrimers with catalytic groups at the core have been synthesized and studied.[23] Placing the catalytic group at the core of the dendrimer allows spatial control of functionalities; this enables steric, photophysical, and electrochemical properties to be controlled. Dendrimers are thus projected as "nanofactories". NCDs fit very well into the concept of nanofactories, and we anticipate that they will have important catalytic applications. This aspect is currently being explored in our laboratory.

Conclusions

This study shows that reduction of hydrogen tetrachloroaurate phase-transferred into toluene in the presence of dendritic polyaryl ether wedges with disulfide groups leads to the formation of nanoparticle-cored dendrimers (NCDs). All evidence suggests that the nanoparticles are structural units of the dendrimer and are not trapped or encapsulated in dendritic pockets. The particles were analyzed by TEM, TGA, UV, IR, and NMR studies, and the results of these studies were consistent with the previously described picture. The density of the branching units connected to the core decreased from 2.18/nm^2 for Au−G-2 to 0.27/nm^2 for Au−G-5. Because of the dendritic structure, these materials enclose large void spaces near the metal cluster, which can act as host cavities for guest molecules. Because a large fraction of the surface area is unpassivated, the core metal cluster may have good catalytic activity. Thus, NCDs can act as hosts as well as catalysts. These properties can make them ideal candidates as nanoreactors. It is proposed that these materials have potential applications in catalysis.

(23) (a) Gitsov, L.; Ivanova, P. T.; Fréchet, J. M. J. *Macromol. Rapid Commun.* **1994**, *15*, 387. (b) Oosterom, G. E.; van Haaren, R. J.; Reek, J. N. H.; Kamer, P. C. J.; van Leeuwen, P. W. N. M. *Chem. Commun.* **1999**, 1119. (c) Brunner, H.; Altman, S. *Chem. Ber.* **1994**, *127*, 2285. (d) Mak, C. C.; Chow, H.-F. *J. Org. Chem.* **1997**, *62*, 5116. (e) Bhyrappa, P.; Young, J. K.; Moore, J. S.; Suslick, K. S. *J. Mol. Catal. A: Chem.* **1996**, *113*, 109. (f) Kimura, M.; Sugihara, Y.; Muto, T.; Hanabusa, K.; Shirai, H.; Kobayashi, N. *Chem.—Eur. J.* **1999**, *5*, 3495. (g) Rheiner, P. B.; Seebach, D. *Chem.—Eur. J.* **1999**, *5*, 3221.

Experimental Section

Chemicals. Benzyl bromide, 3,5-dihydroxybenzoic acid, carbon tetrabromide, triphenylphosphine, 18-crown-6, hydrogen tetrachloroaurate ($HAuCl_4$), tetraoctylammonium bromide (TOAB), and sodium borohydride ($NaBH_4$) were purchased from Aldrich and used as received. Solvents such as toluene, acetone, absolute ethanol, and dichloromethane were obtained from Fisher and used as received. Tetrahydrofuran (THF) was freshly distilled from sodium benzophenone ketyl. Spectroscopic-grade solvents from Aldrich were used for spectral measurements. Water was obtained from a Millipore Nanopure water system.

Synthesis of [G-1]-S. [G-1]-S was prepared from [G-1]-Br. A stirred solution of [G1]-Br (0.5 mM) in freshly distilled THF (5 mL) was cooled to −10 °C, and hexamethyldisilathiane (1.2 equiv) and tetrabutylammonium fluoride (1.1 equiv) were added. The resulting mixture was stirred at room temperature overnight and then was diluted with CH_2Cl_2 (25 mL) and washed with saturated NH_4Cl solution. The CH_2Cl_2 was removed and the residue was chromatographed over silica gel. Elution with CH_2Cl_2 gave the thiol, which was crystallized from a CH_2Cl_2−CH_3OH mixture. Yield, 55%; mp, 89−91 °C. IR: 3061, 3031, 2910, 2869, 1593, 1497, 1451, 1375, 1295, 1159, 1054, 832, 736 cm^{-1}. ^{1}H NMR ($CDCl_3$): δ 3.52 (s, 2 H, C*H*$_2$S), 5.00 (s, 4 H, ArC*H*$_2$O), 6.51−6.58 (m, 3 H, Ar*H*), 7.25−7.40 (m, 10 H, Ph*H*). ^{13}C NMR ($CDCl_3$): δ 43.83 (*C*H$_2$S), 70.32 (*C*H$_2$O), 101.57, 108.75, 127.82, 128.24, 128.83, 137.01, 139.95, 160.19 (Ar*C*). HRMS (FAB) for $C_{42}H_{38}O_4S_2$: calcd, 670.2212; observed, 670.2244.

Synthesis of [G-2]-S. [G-2]-S was prepared from [G-2]-Br by the same procedure as that for [G-1]-S. [G-2]-S was crystallized from a mixture of ether and dichloromethane. Yield, 55%; mp, 141−143 °C. IR: 3061, 3031, 2931, 2873, 1595, 1451, 1375, 1295, 1157, 1052, 832, 736 cm^{-1}. ^{1}H NMR ($CDCl_3$): δ 3.53 (s, 2 H, C*H*$_2$S), 4.91 (s, 4 H, ArC*H*$_2$O), 4.94 (s, 8 H, PhC*H*$_2$O), 6.48−6.59 (m, 9 H, Ar*H*), 7.26−7.36 (m, 20 H, Ph*H*). ^{13}C NMR ($CDCl_3$): δ 43.80 (*C*H$_2$S), 70.19, 70.29 (*C*H$_2$O), 101.82, 106.62, 108.81, 127.85, 128.26, 128.85, 137.07, 139.94, 140.20, 160.08, 160.40 (Ar*C*).

Synthesis of [G-3]-S. [G-3]-S was prepared from [G-3]-Br. Hexamethyldisilathiane (2.4 equiv) and Bu_4NF (2.2 equiv) were used; the components were combined and stirred for 2 d. After the product was subjected to column chromatography, it was dissolved in the minimum quantity of CH_2Cl_2 and ether was added. The product separated as a clear glass, and this material was dried under vacuum at 110 °C for 12 h. Colorless glass, 55% yield. IR: 3060, 3031, 2931, 2873, 1595, 1451, 1374, 1295, 1155, 1052, 832, 736 cm^{-1}. ^{1}H NMR ($CDCl_3$): δ 3.52 (s, 2 H, C*H*$_2$S), 4.81 (s, 4 H, ArC*H*$_2$O), 4.89 (s, 8 H, ArC*H*$_2$O), 4.91 (s, 16 H, ArC*H*$_2$O), 6.50−6.60 (m, 21 H, Ar*H*), 7.20−7.35 (m, 40 H, Ph*H*). ^{13}C NMR ($CDCl_3$): δ 43.83 (*C*H$_2$S), 70.21, 70.33, 70.39 (*C*H$_2$O), 101.89, 106.70, 108.75, 127.88, 128.29, 128.88, 137.09, 139.53, 160.08, 160.33 (Ar*C*).

Synthesis of [G-4]-S. [G-4]-S was prepared from [G-4]-Br in a manner similar to that for [G-3]-S, but 4.8 equiv of hexamethyldisilathiane and 4.4 equiv of Bu_4NF were used. The product was purified several times by dissolving in CH_2Cl_2 and precipitating into ether, then drying at 110 °C under vacuum for 12 h. Colorless glass, 56% yield. IR: 3060, 3032, 2924, 2873, 1595, 1451, 1374, 1295, 1156, 1053, 832, 736 cm^{-1}. ^{1}H NMR ($CDCl_3$): δ 3.52 (s, 2 H, C*H*$_2$S), 4.82 (s, 28 H,

ArCH_2O), 4.91 (s, 32 H, ArCH_2O), 6.48−6.61 (m, 45 H, Ar*H*), 7.25−7.32 (m, 80 H, Ph*H*). ^{13}C NMR ($CDCl_3$): δ 70.12, 70.24 (*C*H_2O), 101.80, 106.62, 127.82, 128.22, 128.80, 137.02, 139.47, 160.24, 160.35 (Ar*C*).

Synthesis of [G-5]-S. [G-5]-S was prepared from [G-5]-Br in a manner similar to that for [G-3]-S, but 9.6 equiv of hexamethyldisilathiane and 8.8 equiv of Bu_4NF were used. The product was purified several times by dissolving in CH_2Cl_2 and precipitating into ether, then drying at 110 °C under vacuum for 12 h. Colorless glass, 59% yield. IR: 3061, 3031, 2918, 2873, 1595, 1451, 1374, 1296, 1155, 1053, 832, 737 cm^{-1}. ^{1}H NMR ($CDCl_3$): δ 3.52 (s, 2 H, C*H*$_2$S), 4.87 (s, 60 H, ArC*H*$_2$O), 4.95 (s, 64 H, ArC*H*$_2$O), 6.49−6.81 (m, 93 H, Ar*H*), 7.25−7.32 (m, 160 H, Ph*H*). ^{13}C NMR ($CDCl_3$): δ 70.20, 70.28 (*C*H_2O), 101.82, 106.63, 127.81, 128.23, 128.78, 128.81, 137.04, 139.48, 160.33 (Ar*C*). Note: The *C*H_2S signal was not observed.

General Procedure for Synthesis of NCDs. To a stirred solution of TOAB (0.342 g, 6.24×10^{-4} M) in toluene (20 mL) was added an aqueous solution of $HAuCl_4$ (0.085 g, 2.5×10^{-4} M) (10 mL) at room temperature. After the solution was stirred for 10 min, the orange toluene layer was separated. To this solution was added a solution of the disulfide (0.1 g for Au−G-1, Au−G-2, and Au−G-3; 0.05 g for Au−G-4 and Au−G-5) in toluene (5 mL). (As seen in Table 3, the number of dendritic wedges attached to each unit surface area of the nanoparticle decreases drastically with an increase in the generation number of the wedge. Thus, the molar ratio of dendrimer/gold required for complete reaction decreases in the series from [G-1]-S to [G-5]-S. In all cases, excess dendritic disulfides present after the reaction were removed by the following protocol.) The mixture was stirred and cooled in ice, and a solution of $NaBH_4$ (0.1 g, 2.5×10^{-3} M) in water (6 mL) was added. The ice bath was removed after 30 min, and stirring was continued for 2 d. The black toluene layer was separated, and the toluene was removed in a rotavapor at 50 °C. The black residue obtained was sonicated with ethanol (20 mL) for 5 min and allowed to settle. The supernatant liquid was decanted. This procedure was repeated (∼20 times) until the supernatant ethanol became clear and colorless immediately after sonication. The ethanol was then decanted and the sample was dried, first in air and then under vacuum for 2 days. The yield of NCDs varied between 20 and 30 mg. To remove TOAB, the samples were placed in an extraction thimble and extracted in a Soxhlet extractor for 4−6 d using ethanol as the solvent. The TOAB could not be completely removed by this procedure. The samples were recovered by dissolving in CH_2Cl_2 and then removing the solvent and repeating the sonication procedure. IR and NMR data for the NCDs are given below. Because the NCD composites contained distributions of particles (see Figure 2), neither elemental analysis nor MALDI spectra provided additional information about purity. Such measurements are also complicated by the tendency of these dendrimers to encapsulate salts and solvents.

Analysis Data for Au−G-1. IR: 3061, 3031, 2910, 2869, 1593, 1497, 1451, 1375, 1295, 1159, 1054, 832, 736. ^{1}H NMR ($CDCl_3$): δ 3.55 (s), 5.00 (s), 6.5 (s), 7.1−7.4 (m). The baseline was not flat, and integrations were not good.

Analysis Data for Au−G-2. IR: 3060, 3031, 2918, 2869, 1595, 1451, 1374, 1295, 1156, 1052, 831, 734. ^{1}H NMR ($CDCl_3$): δ 3.52 (s, 2 H, C*H*$_2$S), 4.91 and 4.93 (s, 12 H, Ar C*H*$_2$O), 6.48−6.62 (m, 9 H, Ar*H*), 7.26−7.35 (m, 20 H, Ph*H*). ^{13}C NMR ($CDCl_3$): δ 44.0 (*C*H_2S), 70.13, 70.24 (*C*H_2O), 101.75, 106.55, 108.73, 127.80, 128.21, 128.79, 136.99, 139.42, 160.01, 160.34 (Ar*C*). Peaks corresponding to TOAB were present in the ^{1}H and ^{13}C NMR spectra.

Analysis Data for Au−G-3. IR: 3061, 3032, 2922, 2873, 1596, 1451, 1374, 1295, 1157, 1053, 832, 736. ^{1}H NMR ($CDCl_3$): δ 3.49 (s, C*H*$_2$S), 4.79−5.01 (m, Ar C*H*$_2$O), 6.44−6.66 (m, Ar*H*), 7.19−7.38 (m, Ph*H*) (the integrations are not very good). ^{13}C NMR ($CDCl_3$): δ 44.0 (*C*H_2S), 70.07, 70.22, 70.32 (*C*H_2O), 101.77, 106.58, 108.80, 127.80, 128.13, 128.78, 136.98, 139.41, 160.19, 160.30 (Ar*C*). Peaks corresponding to TOAB were present in the ^{1}H and ^{13}C NMR spectra.

Analysis Data for Au−G-4. IR: 3061, 3031, 2924, 2872, 1595, 1451, 1374, 1296, 1157, 1054, 832, 736. ^{1}H NMR ($CDCl_3$): δ 4.72−4.93 (m, Ar C*H*$_2$O), 6.44−6.65 (m, Ar*H*), 7.23−7.38 (m, Ph*H*) (the C*H*$_2$S proton was not noticeable, and integrations were not very good). ^{13}C NMR ($CDCl_3$): δ 70.12, 70.22 (*C*H_2O), 101.76, 106.58, 127.77, 128.13, 128.19, 128.72, 128.77, 136.98, 139.42, 160.25, 160.32 (Ar*C*). The *C*H_2S peak was not observed. Peaks corresponding to TOAB were present in the ^{1}H and ^{13}C NMR spectra.

Analysis Data for Au−G-5. IR: 3061, 3031, 2918, 2873, 1595, 1451, 1374, 1296, 1156, 1053, 832, 736. ^{1}H NMR ($CDCl_3$) δ 4.71−4.97 (m, Ar C*H*$_2$O), 6.42−6.64 (m, Ar*H*), 7.22−7.36 (m, Ph*H*) (the C*H*$_2$S proton was not noticeable, and integrations were not very good). ^{13}C NMR ($CDCl_3$): δ 70.11, 70.28 (*C*H_2O), 101.79, 106.59, 127.78, 128.21, 128.79, 136.98, 139.42, 160.25 (Ar*C*). The *C*H_2S peak was not observed. Peaks corresponding to TOAB were present in the ^{1}H NMR spectrum.

Spectroscopy. IR absorbance spectra of drop-cast thin films on KBr plates were acquired using a Nicolet model 510P Fourier transform infrared spectrometer. UV−vis spectra were collected using a Shimadzu model UV-3101PC UV−vis−NIR scanning spectrophotometer. The ^{1}H and ^{13}C NMR spectra of $CDCl_3$ solutions were collected at 400 and 100 MHz, respectively, on a Varian model Mercury 400 spectrometer. The FAB mass spectrum was obtained with a JEOL model HX110HF mass spectrometer. The TGA experiments were performed on a TA Instruments model Hi-Res TGA 2950 thermogravimetic analyzer. High-resolution transmission electron microscopy (HRTEM) images of the particles were obtained with a side-entry Phillips model CM12 electron microscope operating at 120 keV. Samples for TEM were prepared by drop-casting one drop of a ∼1 mg/mL NCD solution in CH_2Cl_2 onto standard carbon-coated Formvar films on copper grids (300 mesh) and drying in air for 30 min. For each sample, two typical regions were scanned. The average cluster diameters were obtained using Scion Image software.

Decomposition by Cyanide. The NaCN-induced decomposition studies of Au−G-*n* were performed as follows. THF solutions of Au−G-*n*, with an optical density in the range of 1−2, were prepared. Samples (3 mL) of these solutions were quickly mixed with 0.5 mL aqueous solutions (10.5 mmol) of NaCN (final [NaCN] = 1.5 mM). The changes in absorbance at 520 nm were monitored for 10 000 s for Au−G-1 and for 1000 s for other NCD generations. The solutions obtained at the end of the experiments were almost colorless.

Acknowledgment. This work was supported by the U. S. Department of Energy, under Grant No. DE-FG02-01ER15280.

JA029544M